NASA TECHNICAL MEMORANDUM

NASA TM X-3169

NASA TM X-3169

EXPERIMENTAL INVESTIGATION OF A SIMPLE DISTORTION INDEX UTILIZING STEADY-STATE AND DYNAMIC DISTORTIONS IN A MACH 2.5 MIXED-COMPRESSION INLET AND TURBOFAN ENGINE

William G. Costakis

Lewis Research Center

Cleveland, Ohio 44135

NATIONAL AERONAUTICS AND SPACE ADMINISTRATION • WASHINGTON, D. C. • JANUARY 1975

1. Report No. NASA TM X-3169	2. Government Accession No.	3. Recipient's Catalog No.
4. Title and Subtitle EXPERIMENTAL INVESTIGATION OF A SIMPLE DISTORTION INDEX UTILIZING STEADY-STATE AND DYNAMIC DISTORTIONS IN A MACH 2.5 MIXED-COMPRESSION INLET AND TURBOFAN ENGINE		5. Report Date January 1975 6. Performing Organization Code
7. Author(s) William G. Costakis		8. Performing Organization Report No. E-8061 10. Work Unit No. 505-05
9. Performing Organization Name and Address Lewis Research Center National Aeronautics and Space Administration Cleveland, Ohio 44135		11. Contract or Grant No. 13. Type of Report and Period Covered Technical Memorandum
12. Sponsoring Agency Name and Address National Aeronautics and Space Administration Washington, D.C. 20546		14. Sponsoring Agency Code
15. Supplementary Notes		

16. Abstract

Steady-state and dynamic distortion data obtained from an inlet-engine compatibility test on a TF30-P-3 engine were used to formulate a simple distortion index that combines steady-state and dynamic distortions. This index correlates well with exhaust nozzle area. Engine tolerance to distortion for different engine bleed configurations was examined.

17. Key Words (Suggested by Author(s))	18. Distribution Statement
Distortion index Dynamic distortion	Unclassified - unlimited STAR Category 02 (rev.)

19. Security Classif. (of this report)	20. Security Classif. (of this page)	21. No. of Pages	22. Price*
Unclassified	Unclassified	21	$3.25

* For sale by the National Technical Information Service, Springfield, Virginia 22151

EXPERIMENTAL INVESTIGATION OF A SIMPLE DISTORTION INDEX UTILIZING STEADY-STATE AND DYNAMIC DISTORTIONS IN A MACH 2.5 MIXED-COMPRESSION INLET AND TURBOFAN ENGINE

by William G. Costakis

Lewis Research Center

SUMMARY

A wind tunnel investigation was conducted to determine the amplitude and spatial distribution of steady-state and dynamic distortion produced in an inlet with 45 percent of the overall supersonic area contraction occurring internally. The inlet support strut location and/or the overboard bypass flow rate had a significant effect on the spatial distribution of distortion. Because of this effect the majority of the stall points exhibited four-per-revolution patterns of distortion.

Data from this test were used to formulate a simple index that combines steady-state and dynamic distortions. Distortion results obtained with this index correlated well with exhaust nozzle area. The exhaust nozzle area of a TF30-P-3, as modified for use in this test, can be controlled in a scheme to avoid engine stall. A considerable increase in engine distortion tolerance can be achieved by opening the 7th-stage bleed. The engine exhibited higher tolerance to distortion for multiple patterns of distortion per revolution than for a one-per-revolution pattern of distortion.

INTRODUCTION

The effect of steady-state total pressure distortion on stall margin has been well documented. In recent years, however, it has become quite apparent that total pressure fluctuations at the compressor face can also alter stall margin. Compressor-face total pressure distortions are a combination of steady-state and dynamic distortions. The manner in which these two types of total pressure distortion combine to affect engine stall margin has become of great interest.

The effect of inlet turbulence on the tolerance of a turbofan engine to steady-state distortion is presented in reference 1. This study shows that steady-state distortion

tolerance decreases as turbulence increases. A procedure for estimating propulsion system flow stability from inlet tests with limited high-response instrumentation is presented in reference 2. In this study the compressor-face average turbulence was transformed into an equivalent square wave pattern having the same effect on stability. Investigations of dynamic distortion from the instantaneous point of view are presented in references 3 to 5.

This present report presents an empirically derived distortion index that combines steady-state and dynamic distortion in the form of rms pressure. A correlation between total pressure distortion, indicated by this index, and exhaust nozzle area is shown. The effect of engine bleed configurations on engine distortion tolerance were also investigated.

This investigation was one part of an overall inlet-engine program using the TF30-P-3 engine with a 55-45 mixed-compression inlet discussed in reference 6. The program also included the implementation of the digital integrated inlet-engine control system discussed in reference 7.

APPARATUS AND PROCEDURE

The propulsion system used in this test consisted of a mixed-compression inlet coupled to a twin-spool turbofan engine. Figure 1 shows a cross section of the inlet and engine installed in the 10- by 10-Foot Supersonic Wind Tunnel.

Inlet

The inlet, shown in figure 2, was designed to operate at a free-stream Mach number of 2.5 with a TF-30 engine. It is an axisymmetric, mixed-compression inlet with 45 percent internal supersonic flow area contraction. Provisions were made for boundary layer bleed on the centerbody and cowl. Cowl bleeds were sealed during the test. The centerbody bleed flow was ducted to four equally spaced support struts located in the diffuser section. Centerbody bleed flow was controlled by a butterfly valve in each strut.

The inlet was equipped with eight overboard bypass doors designed for high-frequency control studies and used to match inlet-engine airflow, as discussed in reference 6. A detailed description of the bypass doors is presented in reference 8. Figure 3 shows a cross section of the diffuser, indicating the circumferential location of the bypass doors and centerbody bleed flow struts. The odd-numbered doors were used

to match airflow to the engine and to induce supercritical inlet conditions for the study of pressure distortions. The even-numbered doors were partially blocked during the test. The total area of the odd-numbered doors was 1610 square centimeters, while the total area of the even-numbered doors was 200 square centimeters. A detailed description of the design of the inlet is given in reference 6.

Engine

The engine used in this investigation was a Pratt & Whitney TF30-P-3. The TF30-P-3 is a mixed-flow, augmented, twin-spool, low-bypass-ratio turbofan engine with a variable-area convergent primary nozzle. The engine consists of a three-stage, axial-flow fan mounted on the same shaft with a six-stage, axial-flow, low-pressure compressor. This unit is driven by a three-stage, low-pressure turbine. The high-pressure spool is a seven-stage, axial-flow compressor driven by a single-stage, air-cooled turbine. The compressor was equipped with low-pressure-compressor (7th stage) and high-pressure-compressor (12th stage) bleeds. The engine was modified (1) by addition of nozzle blockage plates which permitted areas less than 100 percent and (2) by independent control of the engine bleeds. The smallest nozzle area attainable with a standard TF30-P-3 engine is 100 percent.

Instrumentation and Recording Procedure

Figure 4 illustrates the location of pressure instrumentation. The cross section of the inlet shows a plane containing dynamic and steady-state instrumentation at the diffuser exit. A detailed drawing of the diffuser-exit instrumentation is shown in figure 5. The rake assembly consisted of 12 rakes. Each rake consisted of six area-weighted total pressure tubes and three dynamic total pressure transducers. In order to achieve the same area per tube, the angular location of the 12 rakes had to be adjusted for the presence of the four struts. This resulted in a 2.5° shift for the eight rakes adjacent to the struts. The dynamic transducers were subminiature absolute pressure transducers with a flat response in excess of 1000 hertz. The dynamic signals were ac coupled and passed through a second-order filter with a corner frequency of 1000 hertz. The rms value of the fluctuating signals was measured with true rms meters. The steady-state pressures and the output of the rms meters were recorded on a steady-state data recording system.

Test Procedure

The test procedure was designed to cover possible inlet conditions that produce steady-state and dynamic total pressure distortions at the face of the compressor. Figure 6 shows qualitative inlet and fan operating maps indicating the five different inlet conditions examined. The five conditions can be described as follows:

(1) Point 1: The engine was set at a constant corrected speed $N_{l,c}$ and 100 percent exhaust nozzle area. The overboard bypass doors were then varied to create a supercritical inlet condition. The increased dynamic distortion (due to the supercritical inlet condition) combined with steady-state distortion (created by the bypass air) to induce stall.

(2) Point 2: The bypass doors were set at a low setting. Engine corrected speed $N_{l,c}$ was held constant while the exhaust nozzle area was increased. This was an attempt to stall the low-pressure compressor. The exhaust nozzle area was increased to approximately 145 percent of design. When stall did not occur at this point, the bypass doors were opened in order to produce sufficient inlet distortion to induce stall.

(3) Point 3: This point was intended to induce stall in the high-pressure compressor. At a low bypass door setting and constant engine corrected speed $N_{l,c}$ the exhaust nozzle area was decreased to approximately 83 percent. When stall did not occur at this point, the bypass doors were opened in order to increase distortion and induce stall.

(4) Point 4: At a low bypass door setting and 100 percent exhaust nozzle area, engine speed was increased to create a supercritical inlet condition. The resultant increase in dynamic distortion combining with preexisting steady-state distortion induced stall.

(5) Point 5: At 100 percent exhaust nozzle area, engine corrected speed was increased. Then, with engine corrected speed held constant at the increased level, the bypass doors were opened. Stall occurred because of the increased steady-state and dynamic distortions.

These data points were taken with the 7th-stage bleed either open or closed, with zero or some desired angle of attack, and with an optimum or a fully open strut valve configuration. For the optimum strut valve configuration the centerbody bleed flow rate results in a maximum total pressure recovery at design Mach number, design compression ratio, and zero angle of attack. The 12th-stage bleed was open for only one of a total of 33 stall points taken.

All stall points were of the drift type. The procedure was to determine the value of the variable parameter (engine speed or bypass door setting) at stall. The point, then, was repeated with a slightly conservative value for the variable parameter. If stall did not occur within 3 minutes, the data point obtained was considered a nonstall point. The point was then repeated with a variable parameter value closer to the one that caused

stall during the search. Other nonstall points were taken by repeating the data points with a more conservative variable parameter.

The inlet and engine bleed configurations, angle of attack, exhaust nozzle area, and engine corrected speeds for all stall points are shown in table I.

RESULTS AND DISCUSSION

The results presented herein are restricted to the investigation of a simple index suitable for a control signal and are based on a rake differential total pressure and turbulence rms value.

Figure 7 presents the distribution of the rake differential total pressure around the face of the compressor for three operating conditions. The rake differential total pressure is the difference between the compressor-face average total pressure and the rake average total pressure. Figure 7(a) shows a zero-angle-of-attack configuration where the inlet struts and the bypass doors affected the pressure distribution at the diffuser exit. Figure 7(b) shows an angle-of-attack configuration where the pressure distribution was also affected by the inlet struts and the bypass doors. Figure 7(c) shows an angle-of-attack configuration where the pressure distribution apparently was not affected by the struts and the bypass doors.

Steady-state total pressure contour maps for the same stall points shown in figure 7 are presented in figure 8. The contour maps are a result of a computer program which uses the total pressures at the diffuser exit but does not take into consideration the location or the effect of the inlet support struts. The numerical values shown in the figure represent the ratio of the local total pressure to the compressor-face (diffuser exit) average total pressure.

The engine sensitivity to distortion was found to be different for one-per-revolution patterns of distortion than for multiple patterns of distortion per revolution.

The type of distortion pattern obtained was directly related to the bypass door area. Bypass door areas less than 115 square centimeters per door resulted in a one-per-revolution distortion pattern, while larger areas resulted in multiple patterns of distortion per revolution. The most predominant pattern was four per revolution, with the second most predominant being one per revolution.

Because of the rake geometry the smallest increment of the extent of circumferential distortion that could be investigated was assumed to be 30°. Figures 9 and 10 show the relation between exhaust nozzle area and steady-state total pressure distortion. The index used to indicate distortion is the $\left[(\Delta P_{ss})_{min,\,60^{\circ}}\right]/\overline{P}$ index. The subscripts $min, 60^{\circ}$ indicate that the maximum value of the index averaged over a 60° area of

extent is selected. The 60° area of extent was chosen (1) because the average level of distortion for larger extents was too low to be meaningful and (2) because the results obtained for the 60° area of extent were considerably better than those obtained for the 30° area of extent. The steady-state distortion levels indicated by this index do not result in a clear boundary between stall and nonstall points.

Figures 11 and 12 show the results obtained by adding the overall compressor-face average rms value of the fluctuating signal to the steady-state results shown in figures 9 and 10. This correlation is clearly better than that obtained with the steady-state total pressure data alone. However, a distinct boundary still does not exist between all the stall and nonstall points.

The results can be further improved by adding only the average rms value of the fluctuating signals of the worst 60° extent to the corresponding steady-state value. The index then can be expressed as

$$DI60_{ss,rms} = \frac{\left(\Delta P_{ss} + \Delta P_{rms}\right)_{min,\,60^{\circ}}}{\bar{P}}$$

The correlation between distortion indicated by this index and exhaust nozzle area is shown in figures 13 and 14. A fairly clear boundary is now present between the stall and the nonstall regions. These figures indicate that engine tolerance to distortion is higher for multiple patterns of distortion per revolution than for one pattern per revolution. Also, tolerance to distortion decreases considerably when the 7th-stage bleed is closed.

From the control point of view the following observations can be made: Figures 13(a) and (b) indicate that engine tolerance to distortion increases as the exhaust nozzle area increases from 80 percent to 150 percent. No stall points were taken at exhaust nozzle areas below 100 percent for the small bypass door area with 7th-stage bleed open. However, a reasonable interpolation can be made, as shown by the dashed line in figure 13(b). The rate of change in distortion tolerance is greater from 80 percent to 100 percent than from 100 percent to 150 percent of exhaust nozzle area. Thus, through manipulation of exhaust nozzle area, this index can be used in a control system designed to increase engine tolerance to distortion. Figures 14(a) and (b) show that, with 7th-stage bleed closed, the engine tolerance to distortion increases as the exhaust nozzle area increases from 80 percent to 150 percent. However, the rate of increase may be too small to be useful in a control system.

Six steady-state total pressure signals per rake were used in obtaining the results presented in figures 9 to 14. In order to study the effects of using fewer sensors for control purposes, $DI60_{ss,rms}$ was also evaluated using only three steady-state signals per rake. These steady-state signals were the ones corresponding to the three dynamic

signals of each rake. The results are presented in figures 15 and 16. The dashed lines shown in these figures are the stall region boundaries shown in figures 13 and 14. These results are somewhat inferior to those obtained with the higher number of steady-state signals. The small penalty in accuracy, however, may be a justifiable trade-off when a reduced amount of steady-state instrumentation is desirable.

SUMMARY OF RESULTS

An inlet-engine compatibility test was conducted to determine the magnitude and spatial distribution of steady-state and dynamic distortions and their effect on compressor stall. Data from this test were used to formulate a simple distortion index, combining steady-state and dynamic distortion, as a possible control signal. The following results were obtained:

1. The spatial distribution of total pressure was influenced by the strut location and/or the amount of air passed through the bypass doors. High amounts of bypass air resulted in more than one pattern of distortion per revolution, while low amounts of bypass air resulted in one distortion pattern per revolution. This simple relation can be used to determine the type of distortion pattern at the face of the compressor.

2. A distortion index that combines steady-state and dynamic distortions of the same 60° extent was found to correlate very well with exhaust nozzle area. This correlation indicates that this index can be used in a control system designed to increase engine tolerance to distortion.

3. The engine showed somewhat greater tolerance to multiple patterns of distortion per revolution than to one distortion pattern per revolution.

4. Opening the 7th-stage bleed resulted in a considerable increase in distortion tolerance.

5. Reducing the number of steady-state signals by one-half had some effect on the accuracy of the results. The penalty on the accuracy, however, was not large enough to exclude a reduction of steady-state instrumentation, if so needed.

Lewis Research Center,
National Aeronautics and Space Administration,
Cleveland, Ohio, September 24, 1974,
505-05.

APPENDIX - SYMBOLS

A	exhaust nozzle area, cm^2
A^*	design exhaust nozzle area, cm^2
$\frac{A \times 100}{A^*}$	exhaust nozzle area, percent of design
M	Mach number
m	mass flow
N	compressor rotor speed, rpm
N^*	rated compressor rotor speed, rpm
$\frac{N \times 100}{N^* \sqrt{\theta}}$	corrected compressor rotor speed, percent
P	total pressure
$\overline{P}$	average total pressure
ΔP_{rms}	rms value of the fluctuating components of total pressure, N/cm^2
ΔP_{ss}	differential steady-state total pressure, $\overline{P} - P$, N/cm^2
w	engine airflow, kg/sec
α	angle of attack
δ	local corrected total pressure
θ	local corrected total temperature

Subscripts:

c	corrected
h	high-pressure compressor
l	low-pressure compressor
min, 60^o	60^o area of extent with worst distortion
rms	root mean square
ss	steady state
0	free stream
2	compressor face

REFERENCES

1. Van Deusen, E. A.; and Mardoc, V. R.: Distortion and Turbulence Interaction - A Method of Evaluating Engine Inlet Compatibility. J. Aircraft, vol. 9, no. 1, Jan. 1972, pp. 16-22.

2. Ellis, S. H.; and Brownstein, B. J.: A Procedure for Estimating Maximum Time-Variant Distortion Levels with Limited Instrumentation. Paper 72-1099, AIAA, Nov.-Dec. 1972.

3. Costakis, William G.: Analog Computer Implementation of Four Instantaneous Distortion Indices. NASA TM X-2993, 1974.

4. Burstadt, Paul L.; and Calogeras, James E.: Instantaneous Distortion in a Mach 2.5, 40-Percent-Internal-Contraction Inlet and Its Effect on Turbojet Stall Margin. NASA TM X-3002, 1974.

5. Burcham, Frank W., Jr.; and Hughes, Donald L.: Analysis of In-Flight Pressure Fluctuations Leading to Engine Compressor Surge in an F-111A Airplane for Mach Numbers to 2.17. Paper 70-624, AIAA, June 1970.

6. Wasserbauer, Joseph F.; Shaw, Robert J.; and Neumann, Harvey E.: Design of a Very-Low-Bleed Mach 2.5 Mixed-Compression Inlet with 45 Percent Internal Contraction. NASA TM X-3135, 1974.

7. Batterton, Peter G.; Arpasi, Dale T.; and Baumbick, Robert J.: Digital Integrated Control of a Mach 2.5 Mixed-Compression Supersonic Inlet and Augmented Mixed-Flow Turbofan Engine. NASA TM X-3075, 1974.

8. Webb, John A., Jr.; Mehmed, Oral; and Hiller, Kirby W.: Improved Design of High-Response Slotted-Plate Overboard Bypass Valve for Supersonic Inlets. NASA TM X-2812, 1973.

TABLE I. - STALL POINTS

Test run	Steady-state data point reading	Type of stall point	Bypass door setting, cm^2/door	Engine corrected speed, rpm		Angle of attack, α, deg	Exhaust nozzle area, $(A \times 100)/A_8^*$, percent of design	7th-Stage bleed configuration	12th-Stage bleed configuration	Strut valve configuration	Distortion index	
				$N_{l,c}$	$N_{h,c}$						$\frac{(\Delta P_{ss})_{min,60^\circ}}{\bar{P}}$	$\frac{(\Delta P_{ss} + \Delta P_{rms})_{min,60^\circ}}{\bar{P}}$
26	379	1	301	6147	9 626	0	105	Open	Closed	Optimum	0.0526	0.1194
↓	383	1	306	6149	9 621	↓	↓	↓	↓	↓	.0530	.1199
	384	1	301	6143	9 626						.0530	.1192
	389	5	225	6661	9 880						.0535	.1170
27	415	1	177	6005	9 672	2.37					.0790	.1178
27	421	5	132	6456	9 900	2.36					.0770	.1288
31	457	1	69	6007	9 760	3.58				Fully open	.0745	.1043
31	464	5	55	6503	9 994	2.88					.0560	.1003
31	467	5	55	6488	9 984	3.04					.0662	.1109
34	500	4	70	6115	9 768	3.55					.0713	.1080
34	502	4	69	6140	9 788	3.53					.0740	.1122
30	451	1	56	6011	9 604	3.78		Closed			.0474	.0721
31	461	1	78	6031	9 607	2.24					.0378	.0665
35	506	4	69	6223	9 687	2.00					.0334	.0639
36	515	1	140	6145	9 648	0				Optimum	.0454	.0769
27	408	3	241	6204	9 999	0	86	Open			.0341	.0880
30	445	↓	180	6181	10 096	2.38	↓	Open			.0683	.1044
32	474		124	6098	10 080	2.74		Open			.0525	.0892
34	497		112	6123	9 965	2.09		Closed		Fully open	.0339	.0635
27	402	2	216	6895	9 447	0	149	Open		Optimum	.0526	.1303
27	405	↓	225	6879	9 428	0	149	↓		↓	.0534	.1331
29	438		60	6967	9 564	2.38	143				.0679	.1238
29	441		57	6986	9 564	2.38	148				.0619	.1118
33	489	↓	47	6760	9 501	-2.50	149			Fully open	.0712	.1126
36	519	1	387	6345	6 344	0	105		Open	Optimum	.0594	.1328
37	525	↓	330	6350	9 889	0	98		Closed	Optimum	.0539	.1203
37	528		233	7039	9 673	0	128		↓	Optimum	.0603	.1371
38	537		160	6221	9 799	1.56	105	↓		Fully open	.0714	.1230
↓	540	↓	152	6148	9 623	1.55	105	Closed		↓	.0414	.0798
	543	2	200	6997	9 482	↓	147	Open			.0596	.1381
↓	545	2	31	6797	9 380		148	Closed			.0399	.0722
39	561	3	192	6148	10 058		86	Open			.0518	.0890
	568	3	168	6135	9 954	1.54	86	Closed	↓	↓	.0387	.0680

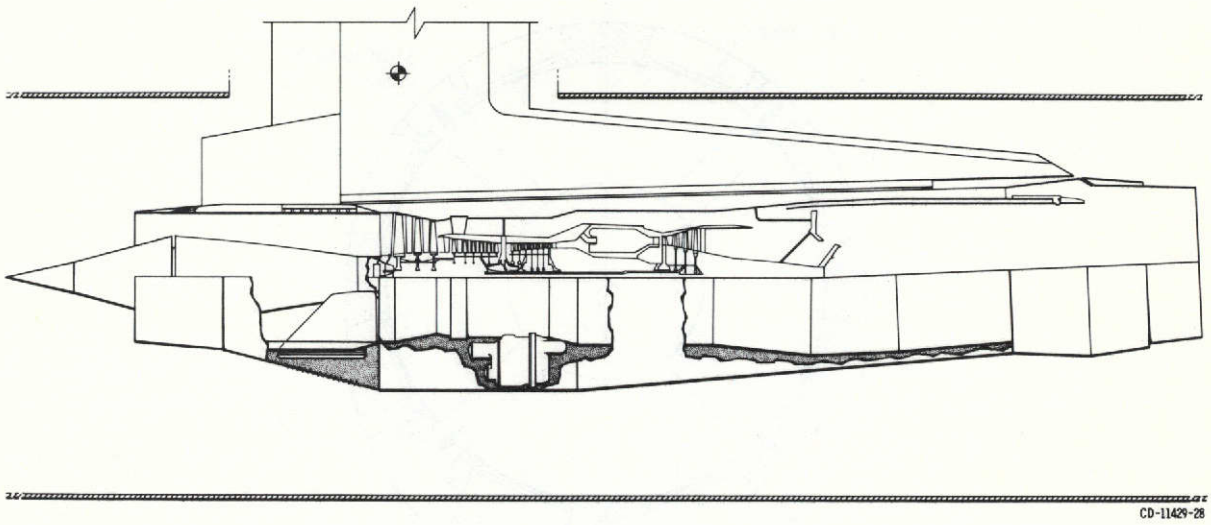

Figure 1. - Cross section of inlet and TF30-P-3 engine installed in 10- by 10-Foot Supersonic Wind Tunnel.

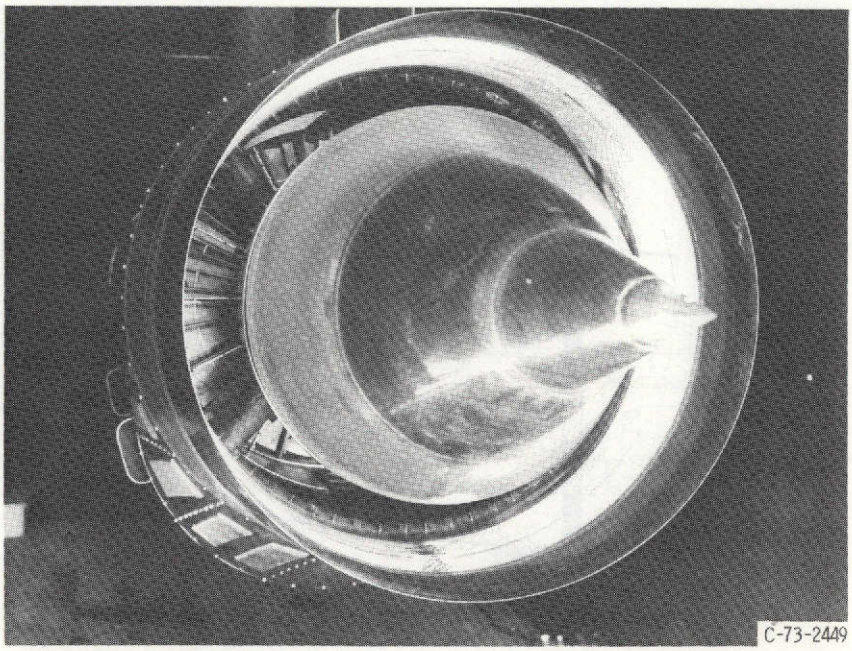

Figure 2. - View down throat of 55-45 inlet showing TF30-P-3 fan.

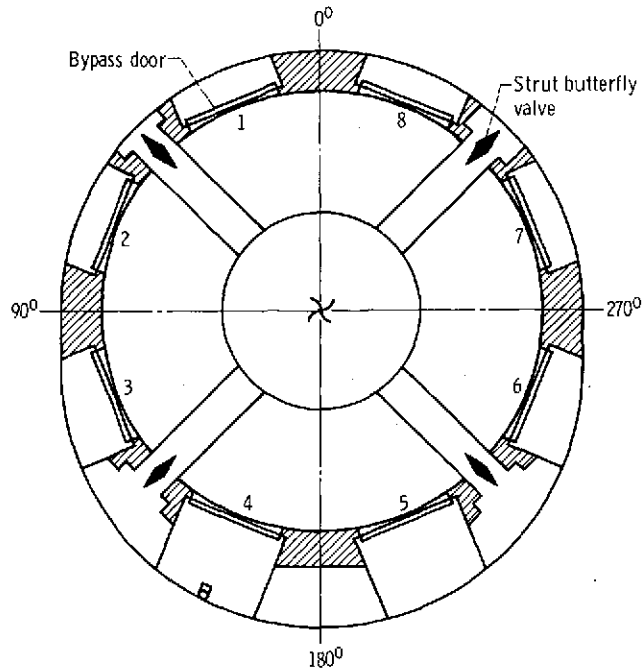

Figure 3. - Cross section of inlet diffuser looking downstream, showing bypass doors and centerbody bleed flow struts.

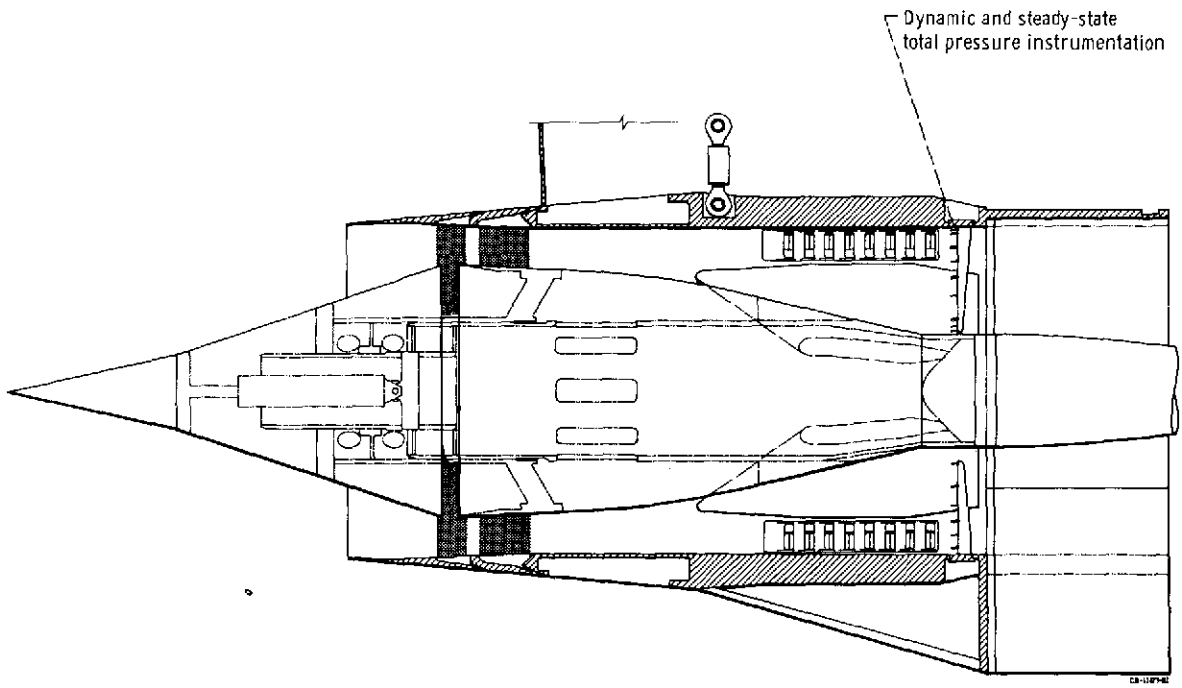

Figure 4. - Cross section of inlet showing instrumentation plane.

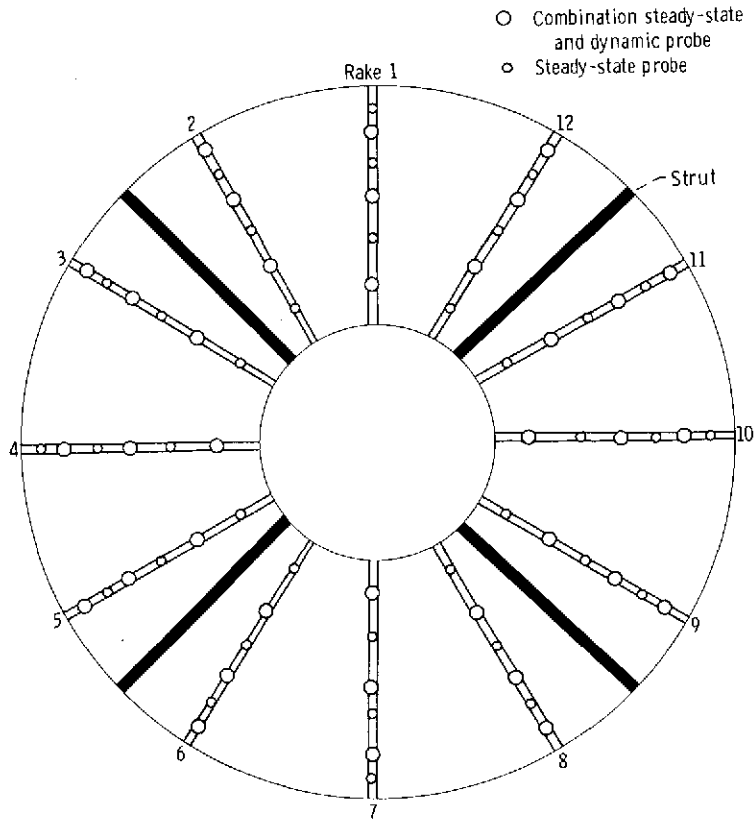

Figure 5. - Compressor-face instrumentation layout, looking downstream.

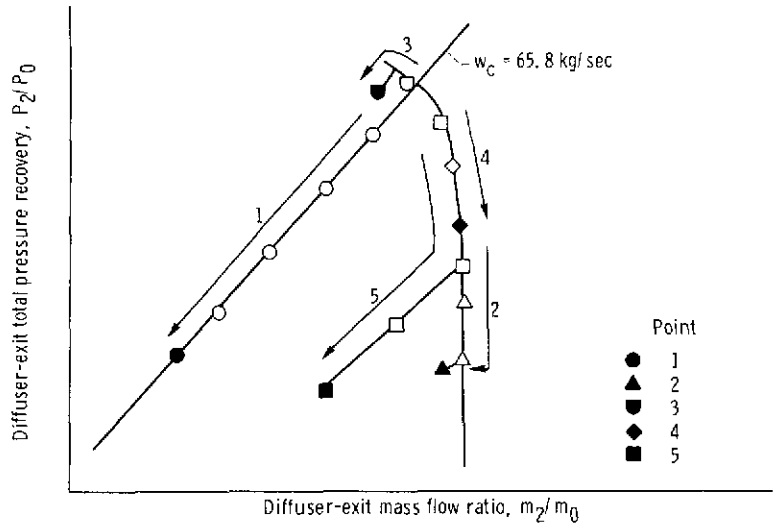

(a) 55-45 inlet operating map.

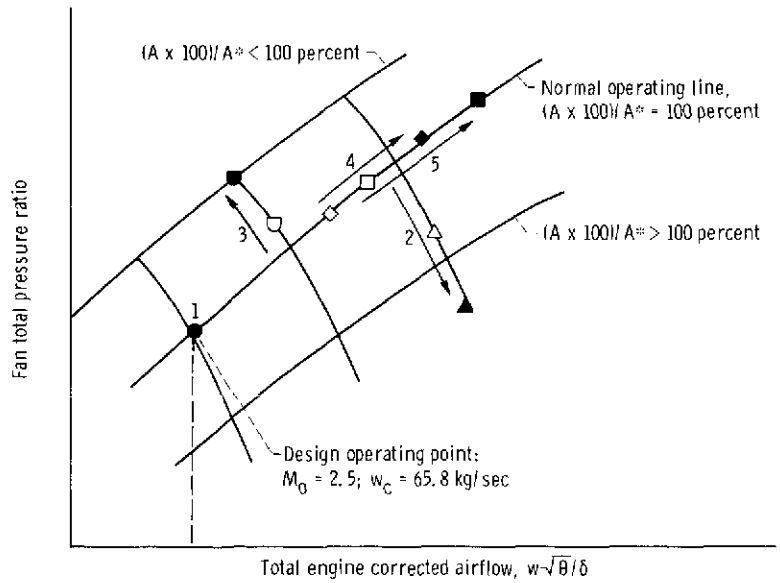

(b) TF30-P-3 fan operating map.

Figure 6. - Types of stall point examined.

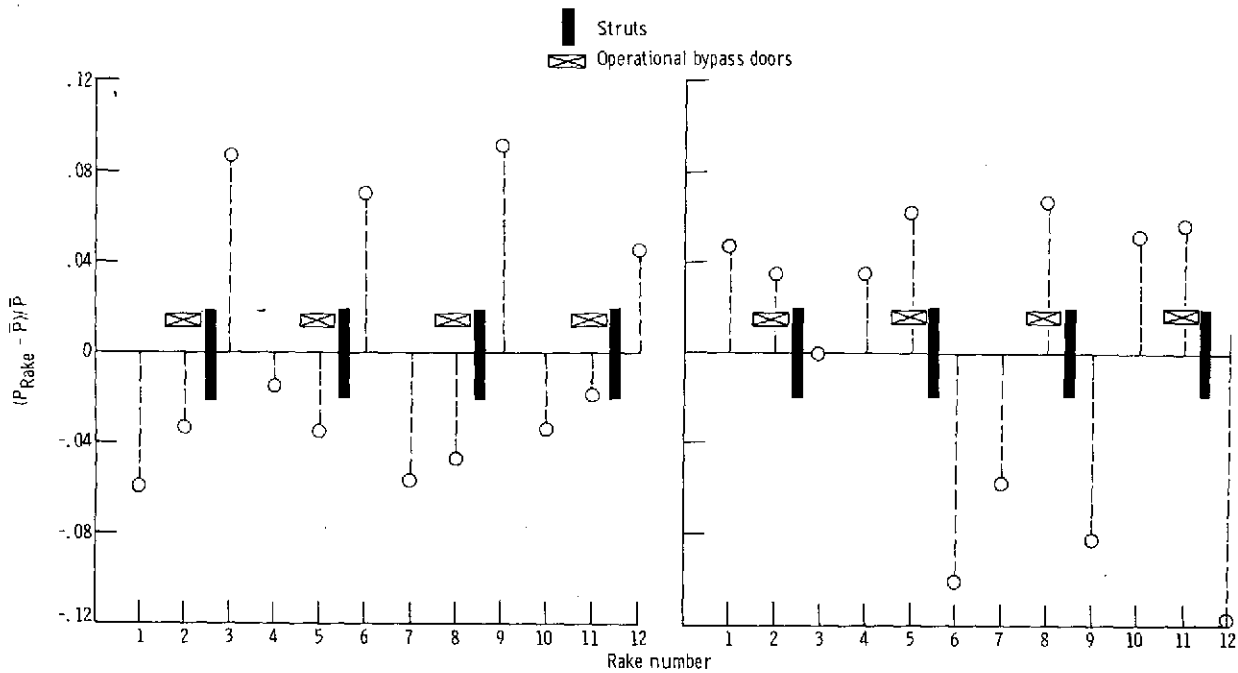

(a) Reading 384; centerbody bleed strut valves in optimum position; 7th-stage engine bleed open; 12th-stage engine bleed closed; bypass door area, 301 cm^2; angle of attack, α, 0^0.

(b) Reading 415; centerbody bleed strut valves in optimum position; 7th-stage engine bleed open; 12th-stage engine bleed closed; bypass door area, 177 cm^2; angle of attack, α, 2.35^0.

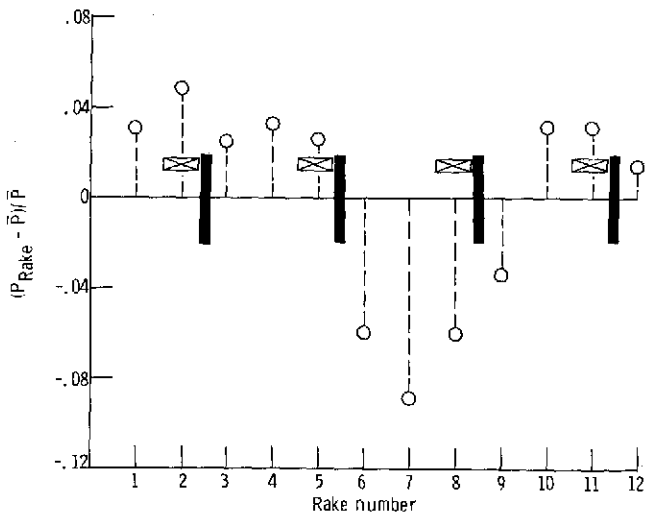

(c) Reading 457; centerbody bleed strut valves in fully open position; 7th-stage engine bleed open; 12th-stage bleed closed; bypass door area, 69 cm^2; angle of attack, α, 9.6^0.

Figure 7. - Rake differential pressure distribution normalized by compressor-face average total pressure.

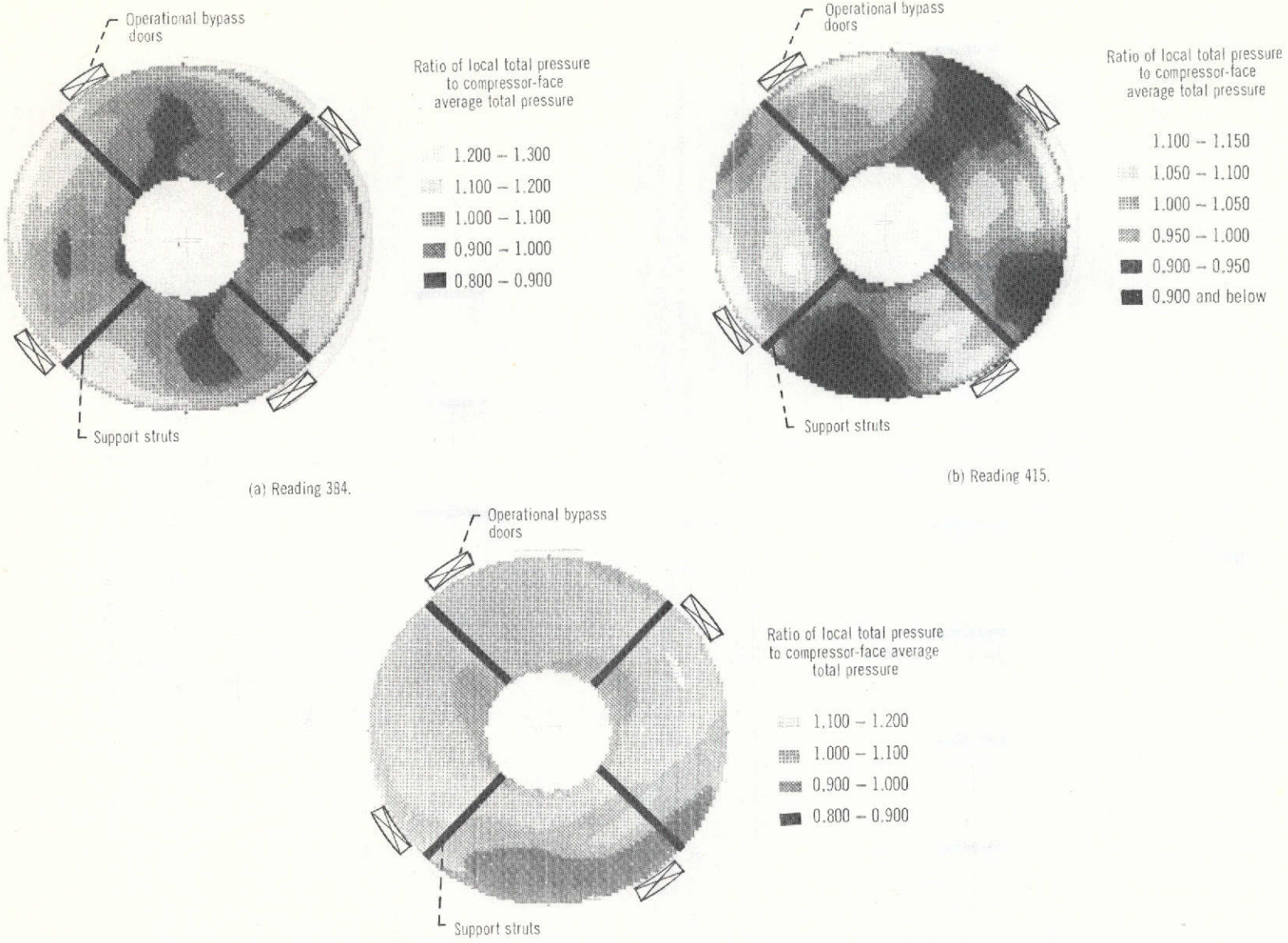

Figure 8. - Compressor-face total pressure contours.

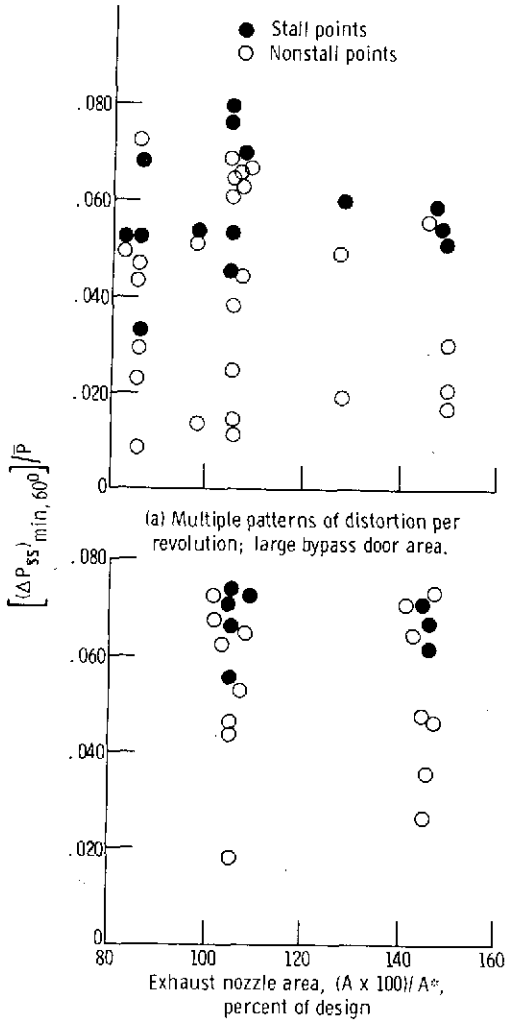

(b) One pattern of distortion per revolution; small bypass door area.

Figure 9. - Relation between nozzle area and steady-state distortion: bleed configuration, 7th stage open and 12th stage closed.

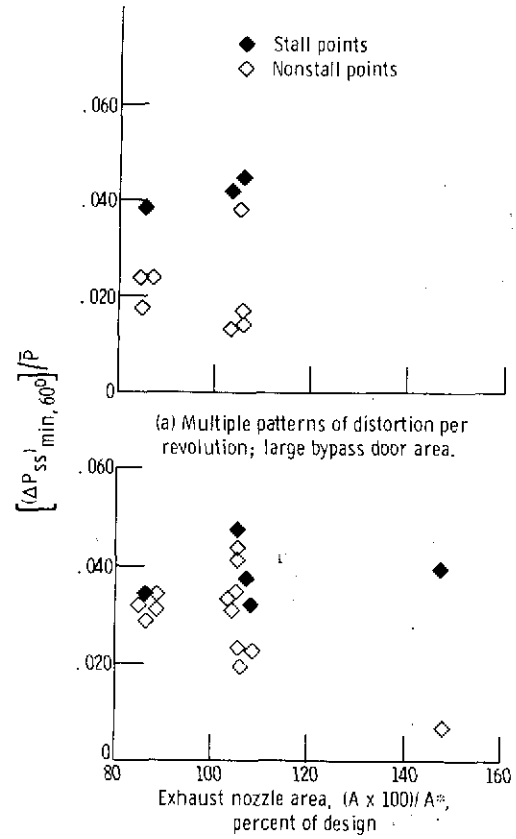

(b) One pattern of distortion per revolution; small bypass door area.

Figure 10. - Relation between nozzle area and steady-state distortion: bleed configuration, 7th stage closed and 12th stage closed.

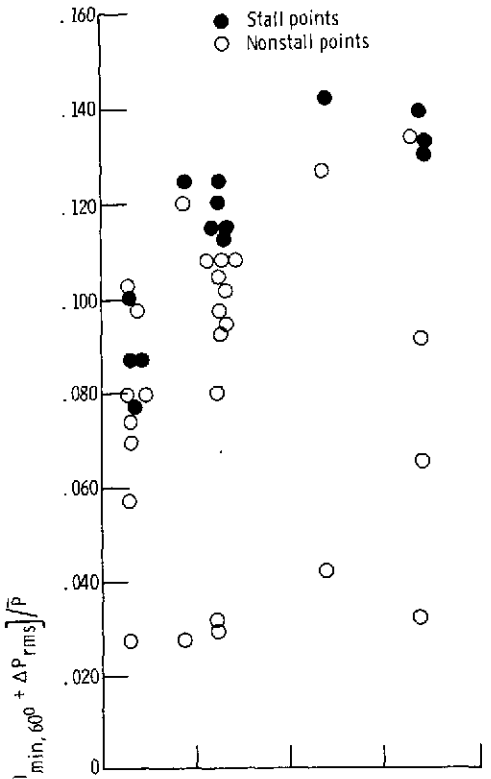

(a) Multiple patterns of distortion per revolution; large bypass door area.

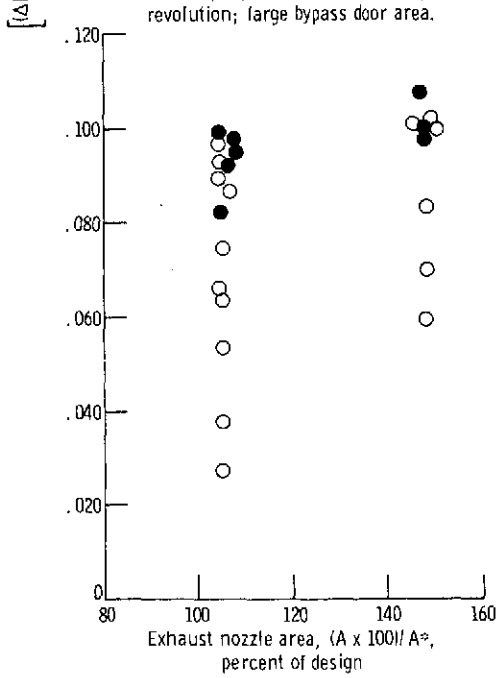

(b) One pattern of distortion per revolution; small bypass door area.

Figure 11. - Relation between nozzle area and distortion: bleed configuration, 7th stage open and 12th stage closed.

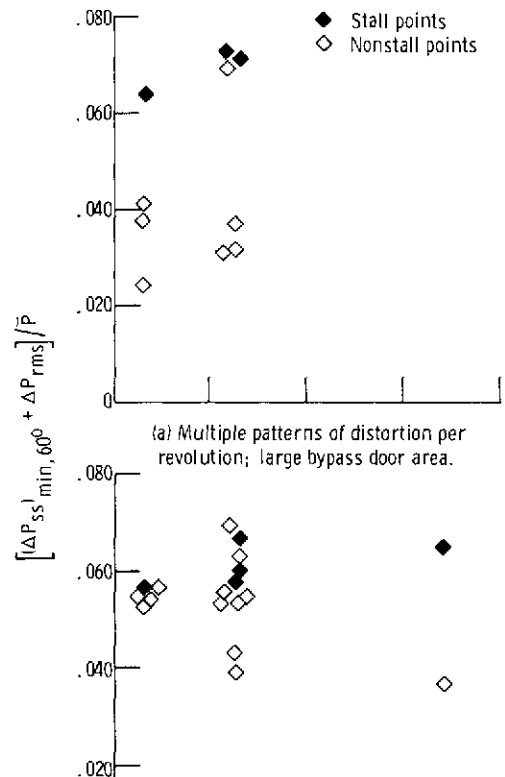

(a) Multiple patterns of distortion per revolution; large bypass door area.

(b) One pattern of distortion per revolution; small bypass door area.

Figure 12. - Relation between nozzle area and distortion: bleed configuration, 7th stage closed and 12th stage closed.

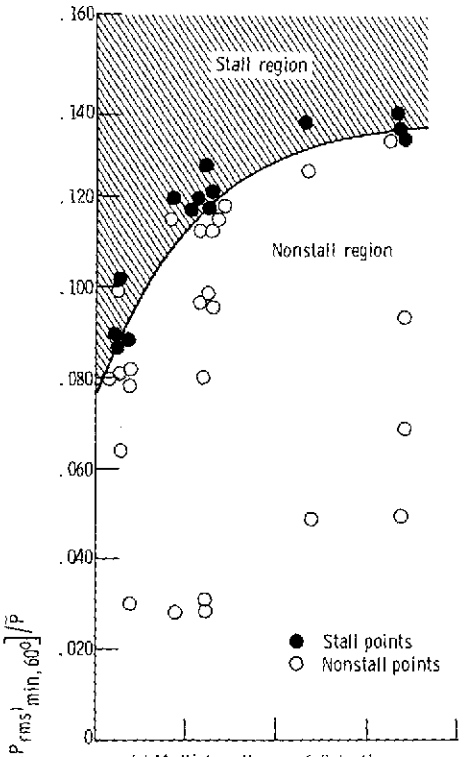

(a) Multiple patterns of distortion per revolution; large bypass door area.

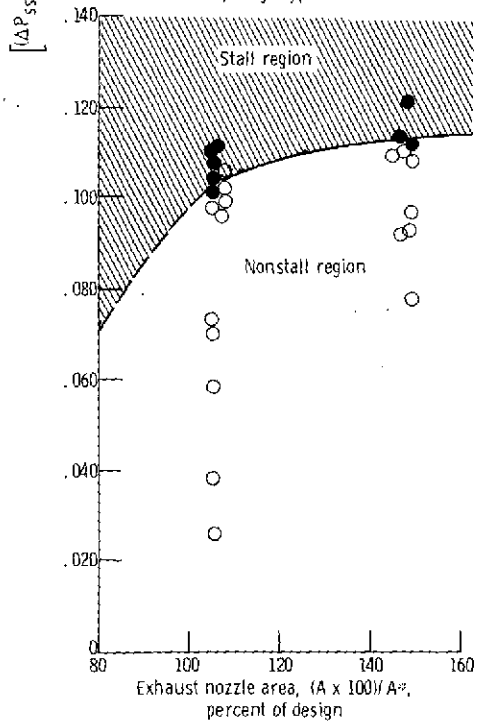

(b) One pattern of distortion per revolution; small bypass door area.

Figure 13. - Relation between exhaust nozzle area and distortion: bleed configuration, 7th stage open and 12th stage closed.

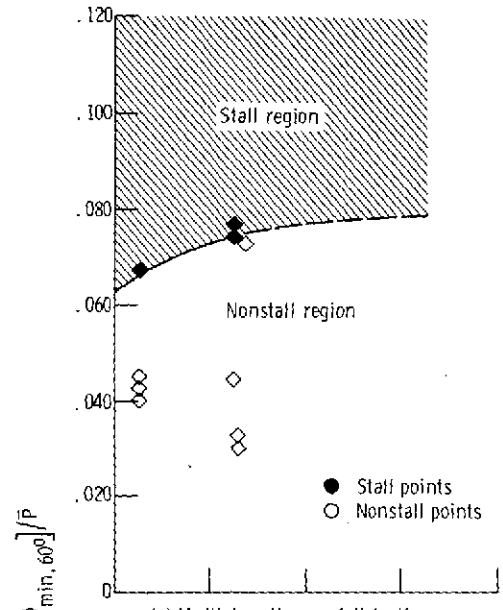

(a) Multiple patterns of distortion per revolution; large bypass door area.

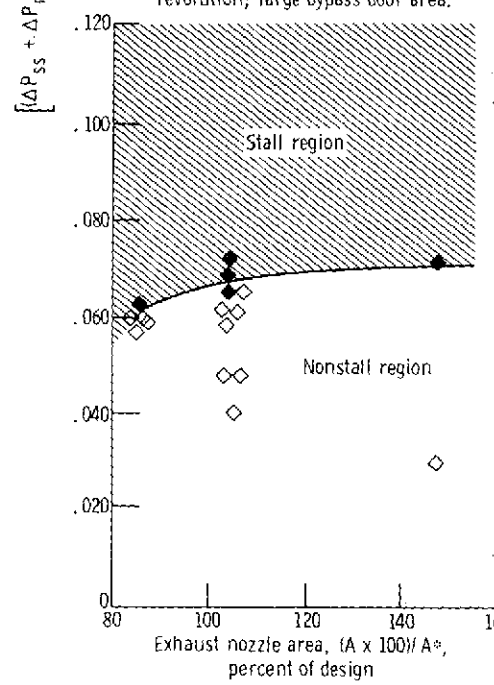

(b) One pattern of distortion per revolution; small bypass door area.

Figure 14. - Relation between exhaust nozzle area and distortion: bleed configuration, 7th stage closed and 12th stage closed.

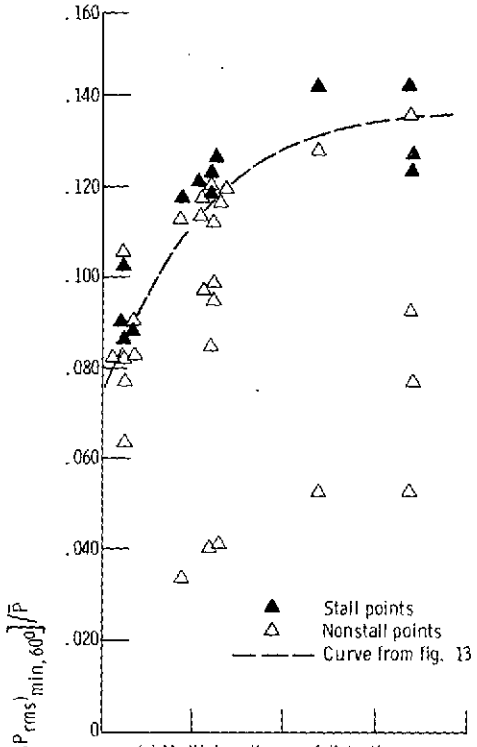

(a) Multiple patterns of distortion per revolution; large bypass door area.

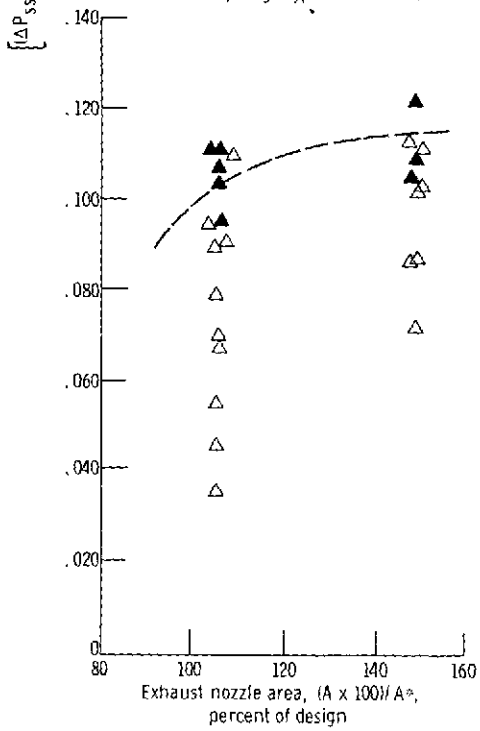

(b) One pattern of distortion per revolution; small bypass door area.

Figure 15. - Relation between exhaust nozzle area and distortion for three steady-state signals per rake: bleed configuration, 7th stage open and 12th stage closed.

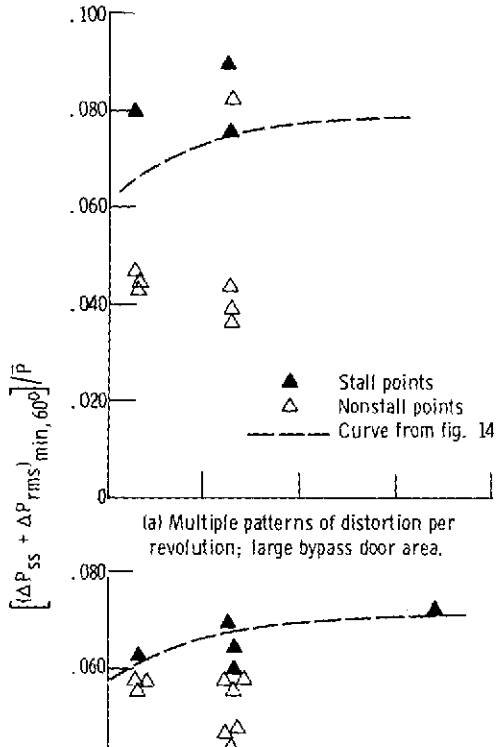

(a) Multiple patterns of distortion per revolution; large bypass door area.

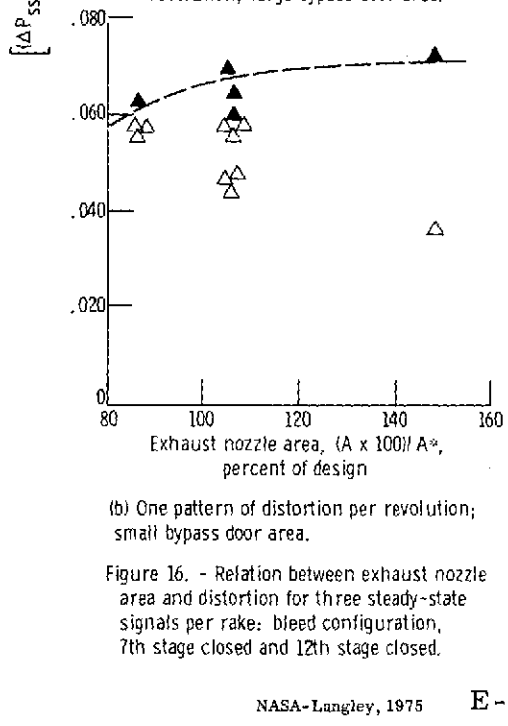

(b) One pattern of distortion per revolution; small bypass door area.

Figure 16. - Relation between exhaust nozzle area and distortion for three steady-state signals per rake: bleed configuration, 7th stage closed and 12th stage closed.

NASA-Langley, 1975 E-8061